

# Study of Geodesics and the Frame-dragging effect in a Rotating Traversable Wormhole

Parthapratiim Pradhan\*

*Department of Physics, Vivekananda Satabarshiki Mahavidyalaya, West Midnapur 721513, India*

Chandrachur Chakraborty†

*Tata Institute of Fundamental Research, Mumbai 400005, India*

## Abstract

The complete equatorial causal geodesic structure of a rotating traversable wormhole is analyzed and it has been shown that the ISCO (Innermost Stable Circular Orbit) coincides at the throat of the wormhole for the retrograde rotation. By studying the effective potential we also find the radius of the circular photon orbit. The Periastron precession frequency and the nodal precession frequency have been derived for both of the direct and retrograde rotation. Moreover, we derive the exact Lense-Thirring precession frequency of a test gyro for the said wormhole and we show that this frequency is inversely proportional to the angular momentum ( $a$ ) of the wormhole along the pole in a certain range of  $r$  ( $r < 16a^2$ ) whereas it is directly proportional to the angular momentum of the spacetime for the other compact objects like black holes and pulsars.

## 1 Introduction

In 1935, Einstein and Rosen first proposed the solutions which involve the mathematical representation of the physical space by a space of two identical sheets, a particle being represented by a ‘bridge’ connecting these sheets [1]. This bridge is now called as “Einstein-Rosen bridge” and the term ‘wormhole’ was first coined by Wheeler in the year 1957 and he also first proposed the concept of the charge-carrying microscopic wormholes [2]. The idea of the traversable wormhole was first given by Morris and Thorne [3] in 1988. It has been shown that to stabilize a traversable wormhole one needs exotic matter with negative energy density [4]. Some simple examples of traversable wormholes were exhibited in [5]. They proved that a traveler can travel in the wormhole without passing through the region of exotic matter [matter violating the weak energy condition (WEC)].

It has also been argued that for the interstellar travel, wormhole could be used as a time machine [4, 6]. The author in [4] argued that to create wormhole it should be needed maximally large curvature which is governed by the laws of quantum gravity. Sometimes it has also been suggested by using quantum foam [2, 7] hypothesis that tiny wormholes might appear and disappear spontaneously at the Planck length [8, 9]. Aspects of quantum or Planck scale Lorentzian wormhole has been suggested in [10, 11] to address the question of quantum gravity effects and the causality violation discussed in [4, 12, 13]. Classical stability of the wormhole has been discussed in [14]. The stable versions of a traversable wormhole indicates as the dark matter candidate [15, 16]. The idea of ‘Inflating Lorentzian wormholes’ discussed in [17]. It has been speculated there that inflation may increase size to the macroscopic wormholes. Time dependence conformal factor may play the key role to expanding the Morris-Thorne wormhole [17, 18, 19]. Two different charged shells could be used as a traversable wormhole connects two asymptotic region without violating the energy condition [20]. The high energy particle collision has been studied by Tsukamoto et al. [21].

---

\*pppradhan77@gmail.com

†chandrachur.chakraborty@tifr.res.in

It may be noted that the traversable wormhole should violate the null energy condition (NEC) at and near the throat, and it is a generic and universal property of wormhole throats[22, 23]. It has been argued that the wormhole throat act as a ‘marginally anti-trapped surface’. They also discussed the ‘Simple flare-out condition’, ‘Strong flare-out condition’, ‘Average flare-out condition’ and ‘N-fold degenerate flare-out condition’ for the dynamic wormholes. By using Raychaudhuri equation and NEC it had been shown that wormhole throat defocused the light rays [24]. Another interesting property, the shadow of a spinning traversable wormhole has been studied by Nedkova et al. [25]. The shadow depends on the angular momentum of the wormhole and the inclination angle of the observer.

Crammer et al. [26] studied the natural wormhole act as the gravitational lenses. They differentiated the lensing pattern of gravitationally negative anomalous compact halo object (GNACHO) and massive compact halo objects (MACHO’s) of positive mass. It has been shown there that how a negative mass object deflected the light rays in the curved space-time (See Fig. 2 in the paper [26]). The light intensity profile of a GNACHO has been studied there (See Fig. 3 in the said references).

Recently, Zhou et al. [27] investigate the possible observational signatures to identify the Ellis wormholes which is basically a massive and compact object. Studying the iron line profile in the X-ray reflected spectrum of a thin accretion disk around the rotating Ellis wormholes they have found some specific observational signatures which can be used to distinguish the wormhole from the Kerr black hole. Thus, there is a possibility to find the wormhole in the near future.

In this article, we have studied the geodesics for the lightlike and timelike region and calculated analytically some observables in the Teo’s rotating traversable wormhole spacetime [28]. We have calculated the Kepler frequency ( $\Omega_\phi$ ) which is proportional to  $r^{-3}$  in Teo’s wormhole but in general it varies with  $r^{-\frac{3}{2}}$  in case of the Kerr black holes and other similar compact objects like pulsars, neutron stars etc. Similarly, the nodal precession frequency and periastron precession frequency are also proportional to  $r^{-3}$  in this case. This can be used to distinguish between a Kerr spacetime and a wormhole spacetime. Another interesting thing is that the ISCO coincides at the throat of Teo’s wormhole for the retrograde rotation. For direct rotation, we could not find the ISCO as the angular momentum vanishes of the test particle. This also leads to vanish the radial epicyclic frequency ( $\Omega_r$ ) in this whole wormhole spacetime. This could be an example of a zero angular momentum observer with a non-vanishing angular velocity ( $\Omega_\phi$ ). This does not happen in the Kerr spacetime as well as some other axisymmetric spacetimes by which we can explain the realistic compact objects of the universe. Interestingly, the Kepler frequency as well as the periastron precession frequency are look alike due to the vanishing radial epicyclic frequency. Thus, we can conclude that Kepler frequency and the Periastron precession frequency are actually same in the Teo’s wormhole. The main interesting thing is that the Lense-Thirring (LT) precession frequency of a test gyro need not to be directly proportional to the rotation of the wormhole always. It may act differently in the wormhole spacetime. In fact, we have shown in this article that the LT precession rate along the pole is inversely proportional to the angular momentum of the wormhole, contrary to our ‘traditional’ thought which tells us that the LT precession rate is not only directly proportional to the rotation of the spacetime but also follow the inverse cube law of the distance. Here, we have also shown that the LT precession rate follows inverse square law along the pole. We suggest that this could make a difference between the wormhole spacetime from the other compact objects for the observational purpose as this highly ‘adverse effect’ has not been found for other spacetimes until now. Thus, our main motivation is to predict some anomalies in the observables for the rotating wormhole spacetime, so that it could be easier to find such an object in our universe by astrophysical observations, if it really exists at all.

The paper is organized as follows : in Sec.2, we investigate the geodesic motion of a test particle in the rotating traversable wormhole. In Sec.2.1, we study the lightlike geodesic and find the radius of the circular photon orbit (CPO). The geodesic motion of a massive test particle has been investigated in Sec.2.2. Sec.3 has been devoted to compute the various observables related to the rotating traversable wormhole as an integral part of the study of geodesics. In Sec.4, we derive the exact Lense-Thirring precession rate of a test gyro which moves in the said wormhole spacetime. Finally, we conclude in Sec.5.

## 2 The Lorentzian traversable wormhole:

In this section, we investigate the complete geodesic structure of the traversable wormhole which is basically described by the metric [28]

$$ds^2 = -N^2 dt^2 + \left(1 - \frac{b}{r}\right)^{-1} dr^2 + r^2 K^2 [d\theta^2 + \sin^2 \theta (d\phi - \omega dt)^2] \quad (1)$$

where  $N, \omega, K, b$  are functions of  $(r, \theta)$  and it is regular on the symmetry axis  $\theta = 0, \pi$ . It indicates two identical, asymptotically flat space-time connected together at the throat  $r = b > 0$ . The discriminant of the metric  $D = g_{t\phi}^2 - g_{tt}g_{\phi\phi} = N^2 K^2 r^2 \sin^2 \theta$  indicates there exist event horizon if  $N = 0$ . Since here  $N \neq 0$  and finite implies that there is no event horizon or no curvature singularity. Here  $b$  is called the shape function that implies  $r \geq b$ .

According to Teo, we can take the parameters  $N$  and  $\omega$  for a particular traversable wormhole as follows:

$$N = K = 1 + \frac{16a^2 d \cos^2 \theta}{r} \quad (2)$$

$$\omega = \frac{2a}{r^3}.$$

where  $b$  and  $d$  [21] are positive constants and the radial coordinate satisfied the condition  $r \geq b$ . The parameter  $a$  is described the total angular momentum of the wormhole. The throat of the wormhole occurs at  $r = b$ . To forming the shape of a wormhole there must be satisfied the ‘flare-out’ condition as

$$\frac{b - b_{,r}r}{2b^2} > 0. \quad (3)$$

The throat of the wormhole looks like a ‘peanut-shell’ like structure (See the figure in the Teo’s [28] work). For fast-rotating wormhole  $a > \frac{b^2}{2}$  and the ergoregion occurs in the range  $b^2 < r^2 < |2a \sin \theta|$ . The ergoregion could not extend to the poles i.e.  $\theta = 0$  and  $\theta = \pi$  but it forms a tube like structure near the equatorial plane.

As we are interested in the complete geodesic structure of this special wormhole (proposed by Edward Teo), without loss of generality we are restricted in the equatorial plane. Thus, the metric reduces to the form

$$ds^2 = -\left(1 - \frac{4a^2}{r^4}\right) dt^2 - \frac{4a}{r} dt d\phi + \left(1 - \frac{b}{r}\right)^{-1} dr^2 + r^2 d\phi^2. \quad (4)$$

To determine the geodesics in the equatorial plane, we shall follow the work of S. Chandrasekar [29]. To compute the geodesic motion of a neutral test particle in this plane we set  $\dot{\theta} = 0$  and  $\theta = \text{constant} = \frac{\pi}{2}$ .

Therefore the necessary Lagrangian for the geodesic motion should be

$$2\mathcal{L} = -\left(1 - \frac{4a^2}{r^4}\right) \dot{t}^2 - \frac{4a}{r} \dot{t} \dot{\phi} + \left(1 - \frac{b}{r}\right)^{-1} \dot{r}^2 + r^2 \dot{\phi}^2 \quad (5)$$

and the generalized momenta can be written as

$$p_t = -\left(1 - \frac{4a^2}{r^4}\right) \dot{t} - \frac{2a}{r} \dot{\phi} = -\mathcal{E} = \text{Const}. \quad (6)$$

$$p_\phi = -\frac{2a}{r} \dot{t} + r^2 \dot{\phi} = \ell = \text{Const}. \quad (7)$$

$$p_r = \left(1 - \frac{b}{r}\right)^{-1} \dot{r} . \quad (8)$$

Here  $(\dot{t}, \dot{r}, \dot{\phi})$  indicates differentiation with respect to affine parameter  $(\tau)$ . Since the Lagrangian does not depend on  $t$  and  $\phi$ , so  $p_t$  and  $p_\phi$  are conserved quantities. The independence of the Lagrangian on  $t$  and  $\phi$  manifested, the stationarity and the axially symmetric character of the wormhole space-time.

Solving Eq. (6) and Eq. (7) for  $\dot{t}$  and  $\dot{\phi}$  we get

$$\dot{t} = \frac{1}{r^2} \left[ \mathcal{E} r^2 - \frac{2a\ell}{r} \right] . \quad (9)$$

$$\dot{\phi} = \frac{1}{r^2} \left[ \frac{2a\mathcal{E}}{r} + \ell \left( 1 - \frac{4a^2}{r^4} \right) \right] . \quad (10)$$

where,  $\mathcal{E}$  and  $\ell$  are the energy and angular momentum per unit rest mass of the test particle.

The normalization of the four velocity( $u^\mu$ ) gives another integral equation for the geodesic motion:

$$g_{\mu\nu} u^\mu u^\nu = \epsilon . \quad (11)$$

or

$$-\mathcal{E}\dot{t} + \ell\dot{\phi} + \frac{\dot{r}^2}{\left(1 - \frac{b}{r}\right)} = \epsilon . \quad (12)$$

where  $\epsilon = -1$  for time-like geodesics,  $\epsilon = 0$  for light-like geodesics and  $\epsilon = +1$  for space-like geodesics.

Substituting these values in equation (12), we obtain the radial equation that governs the geodesic motion of the test particle in the wormhole space-time :

$$\dot{r}^2 = \left(1 - \frac{b}{r}\right) \left[ \mathcal{E}^2 - \frac{4a\ell\mathcal{E}}{r^3} - \frac{\ell^2}{r^2} + \frac{4a^2\ell^2}{r^6} + \epsilon \right] . \quad (13)$$

Using the radial Eq. (13) with the Eqs. (9) and (10) for the other components of the four velocity, we can study many interesting features of the time-like particle and light-like particle in the equatorial plane.

## 2.1 Light-like geodesics:

For null circular geodesics, we have to set  $\epsilon = 0$  and then we find the radial equation:

$$\dot{r}^2 = \left(1 - \frac{b}{r}\right) \left[ \mathcal{E}^2 - \frac{4a\ell\mathcal{E}}{r^3} - \frac{\ell^2}{r^2} + \frac{4a^2\ell^2}{r^6} \right] . \quad (14)$$

To distinguish the geodesics, it is important to introduce the impact parameter  $\eta = \frac{\ell}{\mathcal{E}}$  rather than by  $\ell$ . The equations determining the radius  $r_c$  of the unstable CPO at  $\mathcal{E} = \mathcal{E}_c$  and  $\ell = \ell_c$  by introducing the impact parameter  $\eta_c = \frac{\ell_c}{\mathcal{E}_c}$  are

$$r_c^6 - \eta_c^2 r_c^4 - 4a\eta_c r_c^3 + 4a^2 \eta_c^2 = 0 . \quad (15)$$

$$3r_c^3 - 2\eta_c^2 r_c - 6a\eta_c = 0 . \quad (16)$$

From Eq. (16), we obtain

$$\eta_c = \frac{-3a \pm \sqrt{6r_c^4 + 9a^2}}{2r_c} . \quad (17)$$

Here ‘−’ sign for counter rotating orbit and ‘+’ sign for co-rotating orbit. Inserting Eq. (17) in (15), we find the equation for CPO:

$$r_c^8 - 15a^2r_c^4 \pm (ar_c^4 + 12a^3) \sqrt{6r_c^4 + 9a^2} - 36a^4 = 0. \quad (18)$$

Eliminating square root further we find the CPO equation:

$$r_c^{12} - 36a^2r_c^8 - 1050a^6 = 0. \quad (19)$$

Solving the above equation we get the radius of the CPO as:

$$r_c \approx \pm 2.4626 \sqrt{a}. \quad (20)$$

whereas the upper sign applies to the direct orbits and the lower sign applied to the retrograde orbits.

## 2.2 The Circular time-like Geodesics:

For circular time-like geodesics, Eq. (13) can be written as

$$\dot{r}^2 = \left(1 - \frac{b}{r}\right) \left[ \mathcal{E}^2 - 1 - \frac{4al\mathcal{E}}{r^3} - \frac{\ell^2}{r^2} + \frac{4a^2\ell^2}{r^6} \right]. \quad (21)$$

as  $\epsilon = -1$ .  $\mathcal{E}$  is now to be considered as the energy per unit mass of the particle describing the trajectory. Here the dot indicates derivative with respect to the proper time  $\tau$ .

### (a) Circular orbits:

In this section, we compute the radial equation of ISCO which governing the time-like circular geodesics in terms of reciprocal radius  $u = 1/r$  as the independent variable, may be expressed as

$$\mathcal{B}(u) = u^{-4}\dot{u}^2 = (1 - bu) [4a^2\ell^2u^6 - 4al\mathcal{E}u^3 - \ell^2u^2 + \mathcal{E}^2 - 1]. \quad (22)$$

The conditions for the occurrence of circular orbit are at  $r = r_0$  or the reciprocal radius at  $u = u_0$ :

$$\mathcal{B}(u) = 0. \quad (23)$$

and

$$\mathcal{B}'(u) = 0. \quad (24)$$

Therefore using (22) and (24) we obtain the following equations

$$4a^2\ell^2u_0^6 - 4al\mathcal{E}u_0^3 - \ell^2u_0^2 + \mathcal{E}^2 - 1 = 0 \quad (25)$$

and

$$28a^2\ell^2bu_0^6 - 24a^2\ell^2u_0^5 - 16al\mathcal{E}bu_0^3 - 3\ell^2bu_0^2 + 12al\mathcal{E}u_0^2 + 2\ell^2u_0 + b\mathcal{E}^2 - b = 0. \quad (26)$$

Equations (25) and (26) can be combined to get

$$\frac{\ell_0}{\mathcal{E}_0} = \frac{6au_0}{12a^2u_0^4 - 1}. \quad (27)$$

From Eq. (25) and Eq. (27), we obtain the energy for circular orbit as

$$\mathcal{E}_0 = \frac{1 - 12a^2u_0^4}{\sqrt{1 - 36a^2u_0^4}}. \quad (28)$$

and the angular momentum associated with the circular orbit as

$$\ell_0 = -\frac{6au_0}{\sqrt{1-36a^2u_0^4}}. \quad (29)$$

Surprisingly, angular momentum is negative for the retrograde orbit and it vanishes for the direct orbit which has been discussed in Sec. 5 (see Eq.(59)).

Therefore the minimum radius for a stable circular orbit will be obtained at a point of inflection of the function  $\mathcal{B}(u)$  i.e. we have to supply equations (23) and (24) with the further equation

$$\mathcal{B}''(u) = 0. \quad (30)$$

which gives

$$\frac{\ell_0}{\mathcal{E}_0} = \frac{12au_0(2bu_0 - 1)}{84a^2bu_0^5 - 60a^2u_0^4 - 3bu_0 + 1}. \quad (31)$$

From Eq.(27) and (31), one obtains the ISCO equation for rotating traversable wormhole:

$$36a^2bu_0^5 - 36a^2u_0^4 + bu_0 - 1 = 0. \quad (32)$$

In terms of  $r_0$ , the equation can be rewritten as

$$r_0^5 - br_0^4 + 36a^2r_0 - 36a^2b = 0. \quad (33)$$

interestingly, this equation reduces to a simpler form:

$$(r_0 - b)(r_0^4 + 36a^2) = 0. \quad (34)$$

This indicates that the ISCO occurs at

$$r_0 = r_{ISCO} = b. \quad (35)$$

That means that the *ISCO coincides at the throat* for the *retrograde rotation* in the Teo's wormhole.

#### (b) **Effective Potential:**

One should analyze the stability properties of the geodesic by studying the effective potential [30] due to the geodesic motion of a test particle. For this, we first write the the effective potential for massive particles that governing the radial motion

$$\frac{1}{2} \left( \frac{dr}{d\tau} \right)^2 + \mathcal{V}_{eff} = 0. \quad (36)$$

where the effective potential is given by

$$\mathcal{V}_{eff} = \frac{1}{2} \left( 1 - \frac{b}{r} \right) \left[ 1 - \mathcal{E}^2 + \frac{4a\ell\mathcal{E}}{r^3} + \frac{\ell^2}{r^2} - \frac{4a^2\ell^2}{r^6} \right]. \quad (37)$$

Now let us study the characteristics of the effective potential. Let us choose the value of  $\mathcal{E} = 1$  for simplicity, the effective potential reduces to the following form:

$$\mathcal{V}_{eff} = \frac{\ell}{2r^2} \left( 1 - \frac{b}{r} \right) \left[ \ell + \frac{4a}{r} - \frac{4a^2\ell}{r^4} \right]. \quad (38)$$

It could be seen that the effective potential depends upon the value of throat radius  $b > 0$  and the spin angular momentum parameter  $a$  of the wormhole. Now if we increase the energy of the test

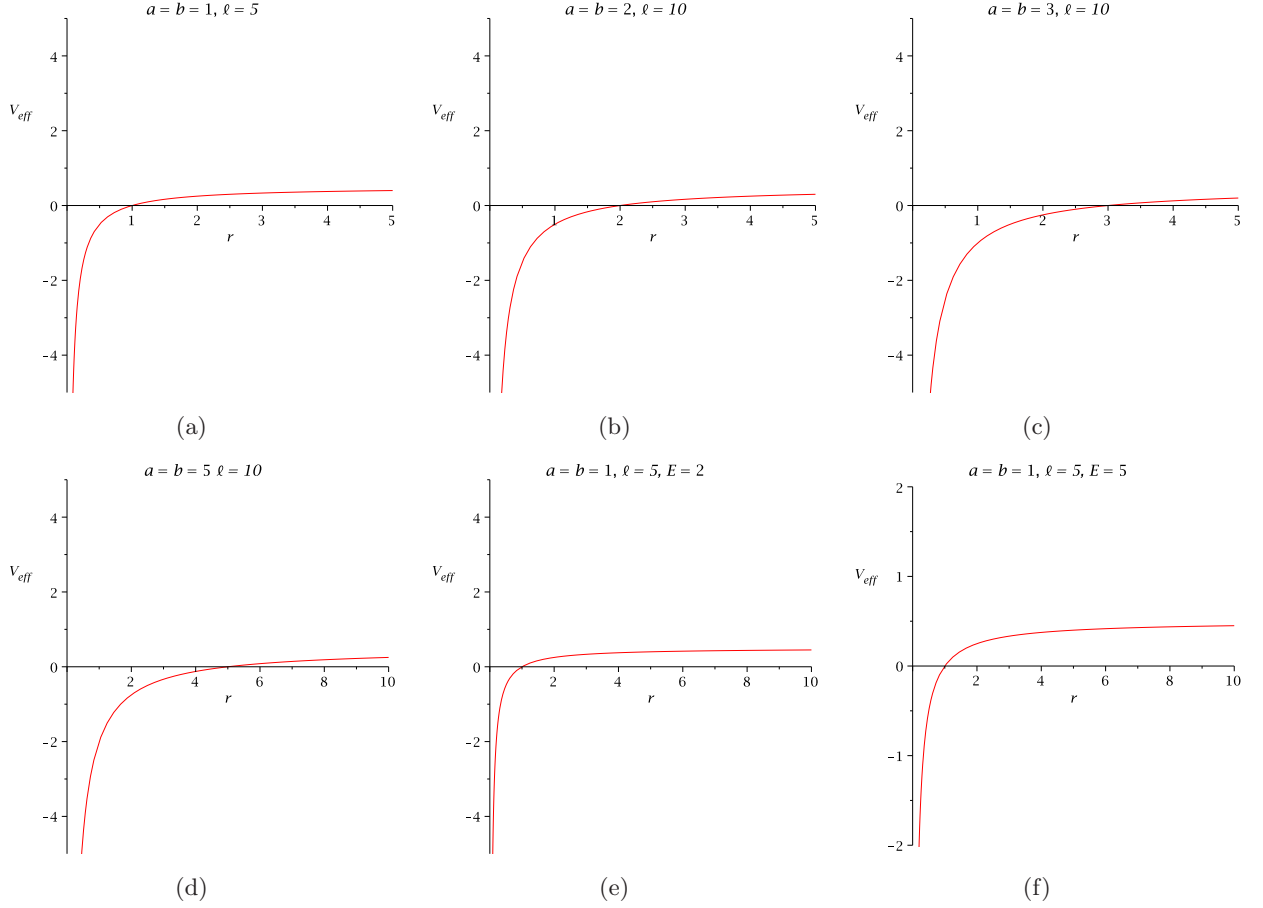


Figure 1: Variation of  $\mathcal{V}_{eff}$  with  $r$  for various values of  $a$ ,  $b$ ,  $\ell$  and  $E$ . One can easily see that  $\mathcal{V}_{eff}$  vanishes at the throat  $r = b$ .

particle the effective potential diagram changes. For example we choose  $\mathcal{E} = 2$ , the effective potential reduces to the following form:

$$\mathcal{V}_{eff} = \frac{1}{2} \left( 1 - \frac{b}{r} \right) \left[ \frac{\ell^2}{r^2} + \frac{8a\ell}{r^3} - \frac{4a^2\ell^2}{r^6} - 3 \right]. \quad (39)$$

In Fig. 1, we have plotted the effective potential with radial coordinate. In this plot, we also show how the effective potential changes with  $r$  for time-like circular geodesics for different values of  $a$  and  $b$  with different values of angular momentum and energy of the test particle.

Now we want to see if we set the value  $r = 1$ ,  $\mathcal{E} = 1$  and  $\ell = 1$ , how the shape of the effective potential changes with  $a$ . In this case  $\mathcal{V}_{eff}$  reduces to the form:

$$\mathcal{V}_{eff} = \frac{(1-b)(1+4a-4a^2)}{2}. \quad (40)$$

If we increase the value of  $\mathcal{E} = 2$  with  $r = 1$ ,  $\ell = 1$ , the expression of  $\mathcal{V}_{eff}$  reduces to

$$\mathcal{V}_{eff} = (1-b)(4a-1-2a^2). \quad (41)$$

We have shown the variation of  $\mathcal{V}_{eff}$  with  $a$  in Fig. 2.

#### (d) **Effective Potential for Photon:**

The radial equation for the light rays is given by

$$\frac{1}{2} \left( \frac{dr}{d\tau} \right)^2 + \mathcal{U}_{eff} = 0. \quad (42)$$

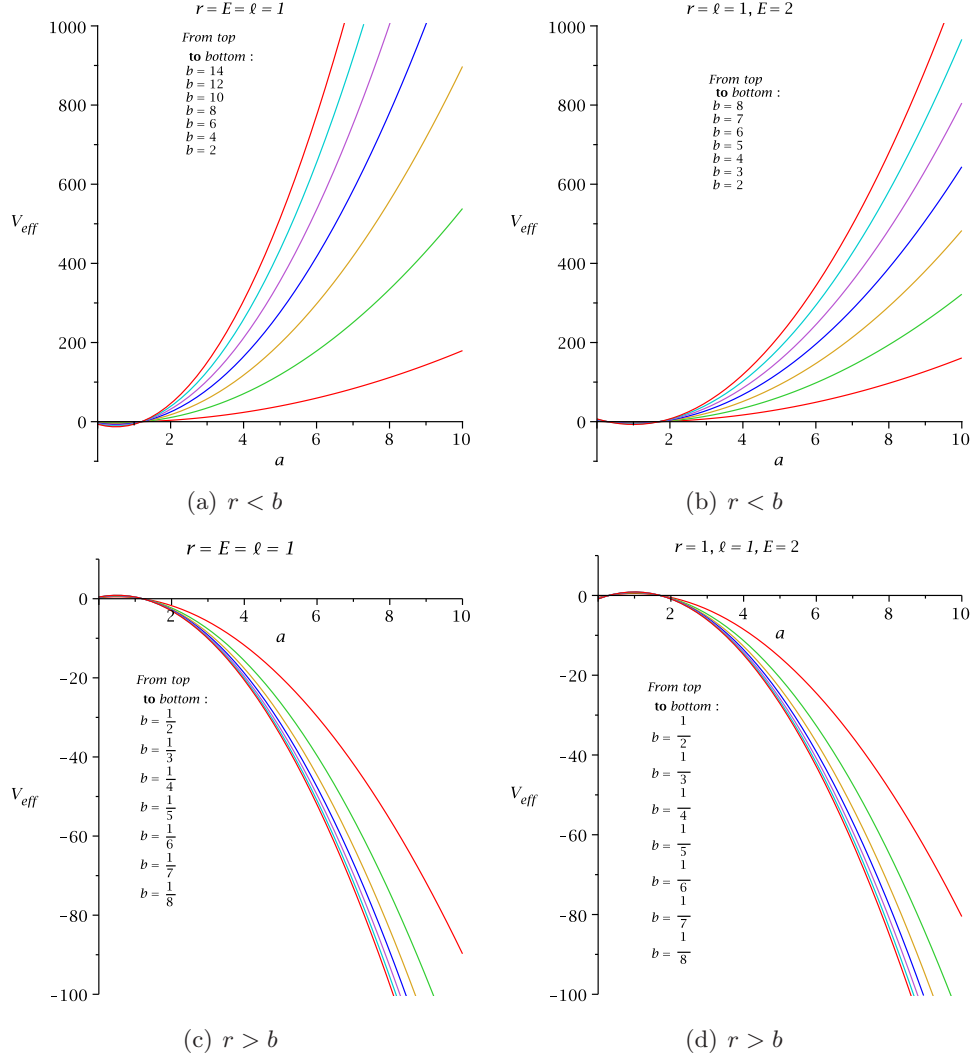


Figure 2: Variation of  $\mathcal{V}_{eff}$  with  $a$  for timelike geodesics.

where the effective potential is defined as

$$\mathcal{U}_{eff} = \frac{1}{2} \left( 1 - \frac{b}{r} \right) \left[ \frac{4a\ell\mathcal{E}}{r^3} + \frac{\ell^2}{r^2} - \frac{4a^2\ell^2}{r^6} - \mathcal{E}^2 \right]. \quad (43)$$

In Fig. 3, we have plotted the effective potential for light rays for various values of energy and angular momentum. For photon's effective potential if we have set  $r = 1$ ,  $\mathcal{E} = 1$  and  $\ell = 1$  then  $\mathcal{U}_{eff}$  reduces to

$$\mathcal{U}_{eff} = 2a(1-a)(1-b). \quad (44)$$

It could be seen from panel (a) and panel (b) of Fig. 4. If the value of angular momentum increases  $\ell = 1$  to  $\ell = 5$  then  $\mathcal{U}_{eff}$  becomes

$$\mathcal{U}_{eff} = 2(1-b)(6 + 5a - 25a^2). \quad (45)$$

and the changes in potential could be seen from panel (c) and panel (d) of Fig. 4. Now, the changes of the value of  $\mathcal{U}_{eff}$  due to increasing the value of energy  $\mathcal{E} = 1$  to  $\mathcal{E} = 5$  can be seen from panel (e) and panel (f) of Fig. 4

$$\mathcal{U}_{eff} = 2(1-b)(5a - a^2 - 6). \quad (46)$$



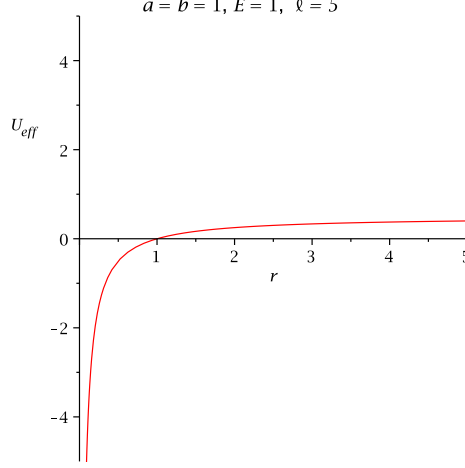


Figure 3: Variation of  $\mathcal{U}_{eff}$  with  $r$  for the lightlike geodesic.

### 3 Observables in the rotating traversable wormhole spacetime

It has already been stated that Zhou et al. [27] recently have studied the X-ray reflected spectrum of a thin accretion disk around the rotating Ellis wormhole which is a massive and compact object. Thus, they have proposed that the wormholes may look like black holes and they have found some specific observational signatures by which it is possible to distinguish rotating wormholes from Kerr black holes. In the case of Teo's traversable wormhole which has been considered in this article, may not be a compact object but if a test particle moves in this wormhole spacetime it experiences some changes in its periodic motion along the various co-ordinates of  $r$ ,  $\theta$  and  $\phi$ . Here, it is necessary to study these periodic variation due to not only the completeness of our study of the geodesic motion of the test particle but also it will help us to derive the orbital plane precession frequency and the periastron precession frequency which is an integral part of the study of geodesics. If it is possible to detect the wormhole in near future and if we want to study some realistic experiment in the rotating wormhole spacetime these precession frequencies may be act as the observables. The periodic motion along  $r$  and  $\theta$  of a test particle are called as radial epicyclic frequency and vertical epicyclic frequency respectively. The periodic variation along  $\phi$  is very well-known to us, which is called as the Kepler frequency.

At first, we should consider a general stationary and axisymmetric spacetime as following

$$ds^2 = g_{tt}dt^2 + 2g_{t\phi}d\phi dt + g_{\phi\phi}d\phi^2 + g_{rr}dr^2 + g_{\theta\theta}d\theta^2 \quad (47)$$

where  $g_{\mu\nu} = g_{\mu\nu}(r, \theta)$ . In this spacetime, the proper angular momentum ( $l$ ) of a test particle can be defined as :

$$l = -\frac{g_{t\phi} + \Omega_{\phi}g_{\phi\phi}}{g_{tt} + \Omega_{\phi}g_{t\phi}} \quad (48)$$

where,  $\Omega_{\phi}$  is the Kepler frequency of the test particle which is defined as [31]

$$\Omega_{\phi} = \frac{d\phi/d\tau}{dt/d\tau} = \frac{d\phi}{dt} = \frac{-g'_{t\phi} \pm \sqrt{g'^2_{t\phi} - g'_{tt}g'_{\phi\phi}}}{g'_{\phi\phi}} \Big|_{r=\text{constant}, \theta=\text{constant}} \quad (49)$$

where the prime denotes the partial differentiation with respect to  $r$ .

For Teo's rotating traversable wormhole (Eq.(4)) we can calculate the Kepler frequency which comes out as,

$$\Omega_{\phi}^d = \frac{2a}{r^3} \quad (50)$$

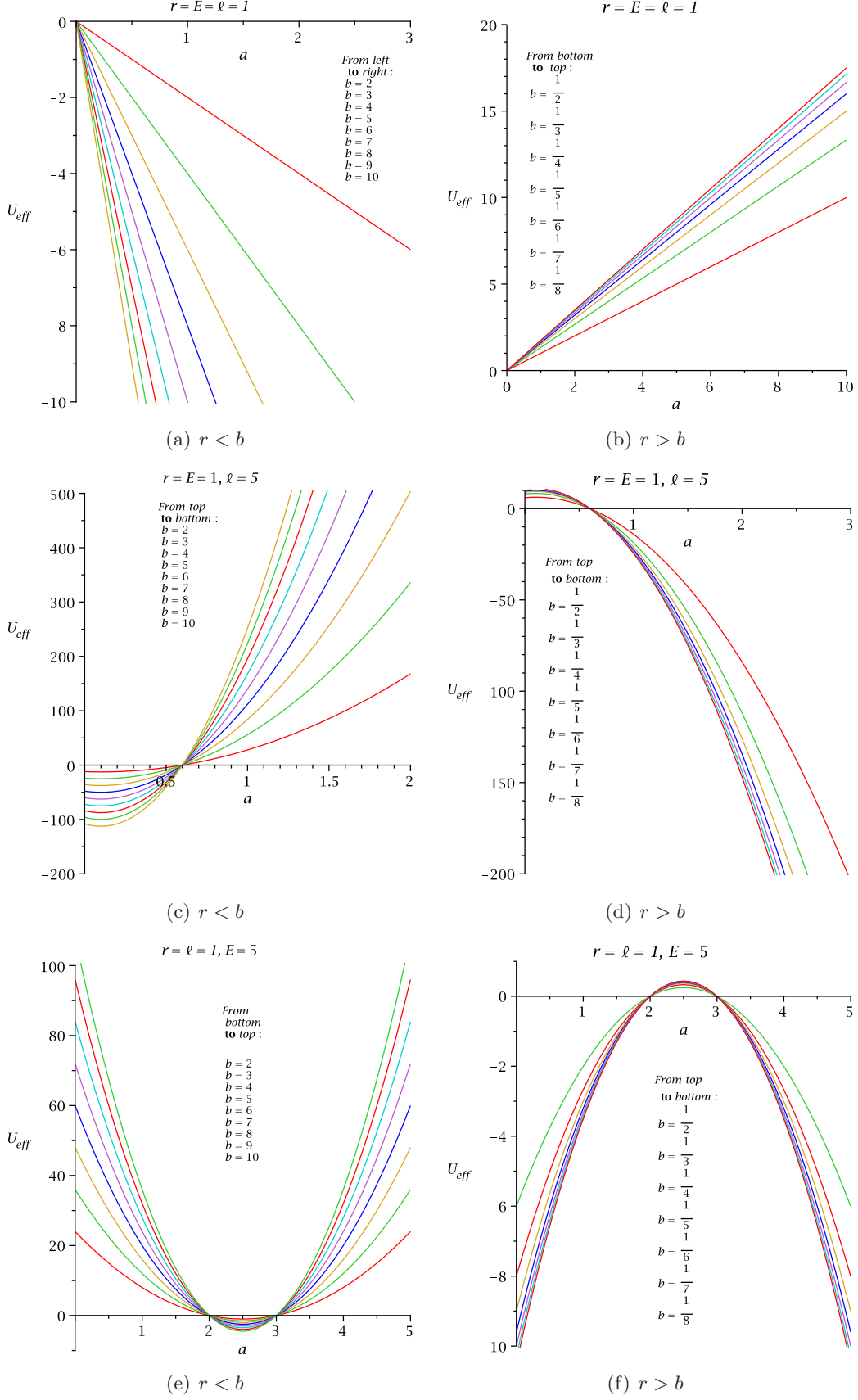


Figure 4: Variation of  $U_{\text{eff}}$  with  $a$  for lightlike geodesics.

and

$$\Omega_\phi^g = -\frac{4a}{r^3}. \quad (51)$$

where the negative sign indicates that the rotation is in the reverse direction. Suffixes  $d$  and  $g$  stand for the direct and retrograde rotation respectively.

The general expressions for calculating the radial ( $\Omega_r$ ) and vertical ( $\Omega_\theta$ ) epicyclic frequencies are [31]

$$\Omega_r^2 = \frac{(g_{tt} + \Omega_\phi g_{t\phi})^2}{2 g_{rr}} \partial_r^2 U \quad (52)$$

$$= \frac{(g_{tt} + \Omega_\phi g_{t\phi})^2}{2 g_{rr}} [\partial_r^2 (g_{\phi\phi}/Y) + 2l \partial_r^2 (g_{t\phi}/Y) + l^2 \partial_r^2 (g_{tt}/Y)]|_{r=const., \theta=const.} \quad (53)$$

and

$$\Omega_\theta^2 = \frac{(g_{tt} + \Omega_\phi g_{t\phi})^2}{2 g_{\theta\theta}} \partial_\theta^2 U \quad (54)$$

$$= \frac{(g_{tt} + \Omega_\phi g_{t\phi})^2}{2 g_{\theta\theta}} [\partial_\theta^2 (g_{\phi\phi}/Y) + 2l \partial_\theta^2 (g_{t\phi}/Y) + l^2 \partial_\theta^2 (g_{tt}/Y)]|_{r=const., \theta=const.} \quad (55)$$

respectively and  $Y$  can be defined as

$$Y = g_{tt}g_{\phi\phi} - g_{t\phi}^2. \quad (56)$$

In our case, we are confined to  $\theta = \pi/2$  which is physically reliable. Thus, we obtain for the Teo's wormhole

$$Y = -r^2 \quad (57)$$

for  $\theta = \pi/2$ . Now, we calculate

$$\partial_r^2 U|_{r=r_{const}, \theta=\pi/2} = \frac{6l}{r^8} (lr^4 - 28a^2l + 8ar^3). \quad (58)$$

As the proper angular momentum are calculated <sup>1</sup> for this particular wormhole as

$$l^d = 0 \quad (59)$$

and

$$l^g = \frac{6ar^3}{12a^2 - r^4} \quad (60)$$

we obtain the radial epicyclic frequencies ( $\Omega_r$ ) from Eq.(53) for the direct and retrograde rotation as

$$\Omega_r^{2(d)} = 0 \quad (61)$$

and

$$|\Omega_r^{2(g)}| = \frac{36a^2 (1 - \frac{b}{r})}{r^{10}} (r^4 + 36a^2) \quad (62)$$

respectively.

---

<sup>1</sup>it has already been calculated in Eq.(27) previously

### 3.1 Periastron precession frequency

It is very surprising that the radial epicyclic frequency vanishes for the direct orbit as the angular momentum is zero in this case. Interestingly, the angular velocity is non zero (Eq.(50)) for the direct orbit which can be an example of the zero angular momentum observer with non-zero angular velocity. Now, we can easily calculate the *periastron precession rate* ( $\Omega_{per}^d$ ) for the direct orbit which turns out to be

$$\Omega_{per}^d = \Omega_\phi^d - \Omega_r^d = \Omega_\phi^d = \frac{2a}{r^3}. \quad (63)$$

Thus, it is really remarkable that the periastron precession rate is equal to the Kepler frequency (Eq.50) for the direct orbit in the Teo's traversable wormhole. But, for the retrograde rotation the *periastron precession frequency* comes out to be

$$\Omega_{per}^g = \Omega_\phi^g - \Omega_r^g = -\frac{2a}{r^3} \left[ 2 + \frac{3}{r^2} \left( 1 - \frac{b}{r} \right)^{\frac{1}{2}} (r^4 + 36a^2)^{\frac{1}{2}} \right]. \quad (64)$$

Negative sign confirms that the rotation is in the reverse direction.

### 3.2 Radius of the ISCOs

It is well-known that the square of the radial epicyclic frequency is equal to zero at the ISCO and it is negative for the smaller radius, which shows the radial instabilities for orbits with radius smaller than the ISCO. In our case, it is easily seen from Eq.(62) that the radius of the ISCO for the *retrograde orbit* is  $b$  which is actually the radius of the throat of the wormhole. Contrary to our case, it has been shown by Zhou et al. [27] that the ISCO radius is at the throat for the *corotating orbit* in the case of Rotating Ellis Wormhole. In the case of Teo's wormhole it has been seen that though the ISCO coincides with the throat for the retrograde rotation, we could not determine the ISCO for the direct orbit as the radial epicyclic frequency as well as the angular momentum of the test particle automatically vanishes for the said wormhole, which is also evident from Eq.(61).

### 3.3 Orbital plane precession frequency

To calculate the orbital plane precession frequency, we first have to obtain the vertical epicyclic frequency for the Teo's wormhole and for that we first calculate

$$\partial_\theta^2 U|_{r=r_{const}, \theta=\pi/2} = \frac{64a^2d}{r} - l \frac{128a^3d}{r^4} + \frac{2l^2}{r^2} \left[ 1 - \frac{32a^2d}{r} \left( 1 - \frac{4a^2}{r^4} \right) \right]. \quad (65)$$

Now, substituting it into Eq.(55) and also taking the values of  $l$  from Eq.(59,60) we obtain

$$\Omega_\theta^2 (d) = \frac{32a^2d}{r^3} \quad (66)$$

for the direct orbit and for the retrograde orbit we obtain

$$\Omega_\theta^2 (g) = \frac{4a^2}{r^7} [9r + 8d(r^4 - 36a^2)]. \quad (67)$$

As it have already been derived the exact Kepler frequencies and the vertical epicyclic frequencies of a test particle which rotates in a circular orbit around the traversable wormhole in the equatorial plane, now we can obtain the *nodal precession rate* ( $\Omega_{nod}$ ) easily. It is also called as the orbital plane precession frequency or the LT precession frequency for a *test particle*. Using Eq.(50,51) and Eq.(66,67) we obtain :

$$\Omega_{nod}^d = \Omega_\phi^d - \Omega_\theta^d = \frac{2a}{r^3} (1 - \sqrt{8r^3d}) \quad (68)$$

for the direct orbit and for the retrograde orbit it comes out to be

$$\Omega_{nod}^g = \Omega_\phi^g - \Omega_\theta^g = -\frac{2a}{r^3} \left[ 2 + \left( 9 + \frac{8d}{r}(r^4 - 36a^2) \right)^{\frac{1}{2}} \right] \quad (69)$$

where the negative sign indicates that the rotation is in the reverse direction. Both of the nodal frequencies are proportional to  $a$  as well as  $r^{-3}$  which is expected.

## 4 Lense-Thirring precession of a test gyro moving in the rotating traversable wormhole spacetime

We are keen to derive the Lense-Thirring precession [32] frequency of a test gyro [33] in a general rotating traversable wormhole spacetime, which could be regarded as a more realistic observable for the indirect detection of a wormhole. In 2004, NASA had sent the Gravity Probe B (GP-B) satellite to measure the Geodetic and LT precession frequencies of a test gyro due to the rotation of the earth and the result had been published by Everitt et al. in 2011 [34]. It may play an important role in the future astrophysical observational purpose to measure the LT precession frequency of a wormhole to distinguish its nature from the other compact objects as well. Perhaps Chakraborty and Majumdar [35] first derived the exact LT precession rate of a test gyro in the Kerr spacetime [35] and some other axisymmetric spacetimes [36, 37]. Now, the same formulation can also be applied to obtain the frame-dragging effect in the case of rotating wormhole as well. The canonical metric for a general stationary, axisymmetric traversable wormhole has been written in Eq.(1). Using this metric, the exact Lense-Thirring precession rate of the rotating wormhole can be expressed in the orthonormal coordinate basis as:

$$\begin{aligned} \vec{\Omega}_{LT} = & \frac{1}{2NK(-N^2 + \omega^2 r^2 K^2 \sin^2 \theta)} \cdot \\ & \left[ K \left( 1 - \frac{b}{r} \right)^{1/2} \sin \theta [N^2(Kr\omega_{,r} + 2\omega r K_{,r} + 2\omega K) + \omega^2 r^3 K^3 \omega_{,r} \sin^2 \theta - 2\omega K r N N_{,r}] \hat{\theta} \right. \\ & \left. + [N^2(K\omega_{,\theta} \sin \theta + 2\omega K_{,\theta} \sin \theta + 2\omega K \cos \theta) + \omega^2 r^2 K^3 \omega_{,\theta} \sin^3 \theta - 2\omega K N N_{,\theta} \sin \theta] \hat{r} \right] \end{aligned} \quad (70)$$

and the modulus of the above LT precession rate is

$$\begin{aligned} \Omega_{LT} = & |\vec{\Omega}_{LT}(r, \theta)| \\ = & \frac{1}{2NK(-N^2 + \omega^2 r^2 K^2 \sin^2 \theta)} \cdot \\ & \left[ K^2 \left( 1 - \frac{b}{r} \right) \sin^2 \theta [N^2(Kr\omega_{,r} + 2\omega r K_{,r} + 2\omega K) + \omega^2 r^3 K^3 \omega_{,r} \sin^2 \theta - 2\omega K r N N_{,r}]^2 \right. \\ & \left. + [N^2(K\omega_{,\theta} \sin \theta + 2\omega K_{,\theta} \sin \theta + 2\omega K \cos \theta) + \omega^2 r^2 K^3 \omega_{,\theta} \sin^3 \theta - 2\omega K N N_{,\theta} \sin \theta]^2 \right]^{\frac{1}{2}} \end{aligned} \quad (71)$$

In this present paper we have studied the geodesics of a special wormhole (Eq.4) choosing some specific function of the metric components (Eq.3) which is basically first taken by E. Teo.

### 4.0.1 LT precession in Teo's wormhole: LT precession frequency is inversely proportional to the angular momentum of the wormhole spacetime along the pole

According to Teo, we can take  $N$  and  $\omega$  as the following:

$$N = K = 1 + \frac{16a^2 d \cos^2 \theta}{r}, \quad \omega = \frac{2a}{r^3} \quad (72)$$

and we can calculate the exact LT precession rate of a test gyro for the said wormhole which can be expressed as

$$\vec{\Omega}_{LT} = \frac{a}{Nr^3 \left(1 - \frac{4a^2}{r^4} \sin^2 \theta\right)} \cdot \left[ N \sin \theta \left(1 - \frac{b}{r}\right)^{\frac{1}{2}} \left(1 + \frac{12a^2}{r^4} \sin^2 \theta\right) \hat{\theta} - 2 \cos \theta \hat{r} \right]. \quad (73)$$

Along the pole we can take  $\theta = 0$  and obtain the LT precession rate as

$$|\vec{\Omega}_{LT}| = \frac{2a}{r^2(r + 16a^2d)}. \quad (74)$$

and along the equator we take  $\theta = \pi/2$  and the LT precession rate comes out as

$$|\vec{\Omega}_{LT}| = \frac{a}{r^3 \left(1 - \frac{4a^2}{r^4}\right)} \cdot \left(1 - \frac{b}{r}\right)^{\frac{1}{2}} \left(1 + \frac{12a^2}{r^4}\right) \hat{\theta}. \quad (75)$$

In weak field approximation ( $a \ll r^2$ ) Eq.(73) reduces to

$$\vec{\Omega}_{LT} = \frac{a}{Nr^3} \cdot \left[ N \sin \theta \left(1 - \frac{b}{r}\right)^{\frac{1}{2}} \hat{\theta} - 2 \cos \theta \hat{r} \right] \quad (76)$$

It should be important to mention here that as the LT precession formulation is valid only outside the ergoregion, Eq.(73) and the related equations will be valid only in the following range:

$$r > b \quad \text{and} \quad r^2 > 2a \sin \theta \quad (77)$$

and both of the above conditions must be hold. As we have stated earlier that the ergoregion occurs for the rotating Teo's wormhole in this range  $b < r < \sqrt{2a \sin \theta}$ , the calculation of LT precession frequency is valid only for  $r > \sqrt{2a \sin \theta}$ . It should be noticed that the ergoregion does not fully surround the throat but forms a tube around the equatorial region of the said wormhole. Unlike a rotating black hole spacetime, the ergoregion of a rotating wormhole does not coincide with the horizon at the pole as the event horizon does not exist in this spacetime at all. At the equatorial plane, the ergoregion is extended upto  $r = \sqrt{2a}$  and it decreases slowly if we move to the pole from the equator. Finally, the ergoregion vanishes ( $r = 0$ ) at the pole for  $\theta = 0$ .

We have plotted (Fig.5) the LT precession frequencies (73) of the Teo's wormhole to see the graphical nature of it. It can be seen from panel (a) of Fig.5 that the LT precession frequency ( $\Omega_{LT}$ ) decreases along the pole with increasing the angular momentum ( $a$ ) of the spacetime (Red, Green and Blue stand for  $a = 10, a = 15$  and  $a = 20$  respectively). This is remarkable in this sense that the LT precession frequency varies inversely with the rotation of the spacetime or so-called the angular momentum of the spacetime. Generally, frame-dragging rate varies directly with  $a$  in the case of the black holes and pulsars but in the case of wormhole it behaviour is slightly different. The evolution of the frame-dragging rate has been shown in panel (a)-(f) of Fig.5. If we move from the pole to the equator, the blue line comes upward in a faster rate than the red one and the three colours are indistinguishable in panel (b) and panel (c) for choosing the particular range of  $r$ . After crossing the angle  $\sim 10^0$  with respect to the pole, the three colours are distinguishable and we can see that red line comes down and blue line comes up which is *more physical* as it was known to us till now that if we increases the rotation of the spacetime frame-dragging rate increases. In this sense, panel (d)-(f) are not surprising but the nature of the plots of panel (a)-(c) is quite unexpected to us. Frame-dragging behaves differently only along the pole and its nearby region ( $\sim 10^0$ ) in the *rapidly rotating* ( $r \sim \sqrt{a}$ ) wormhole spacetime. In the case of the slow rotation, it does not behave differently along the pole, we mean, the frame-dragging rate decreases with decreasing the rotation of the spacetime not only along the pole but also along the equator of this wormhole spacetime like the other compact objects

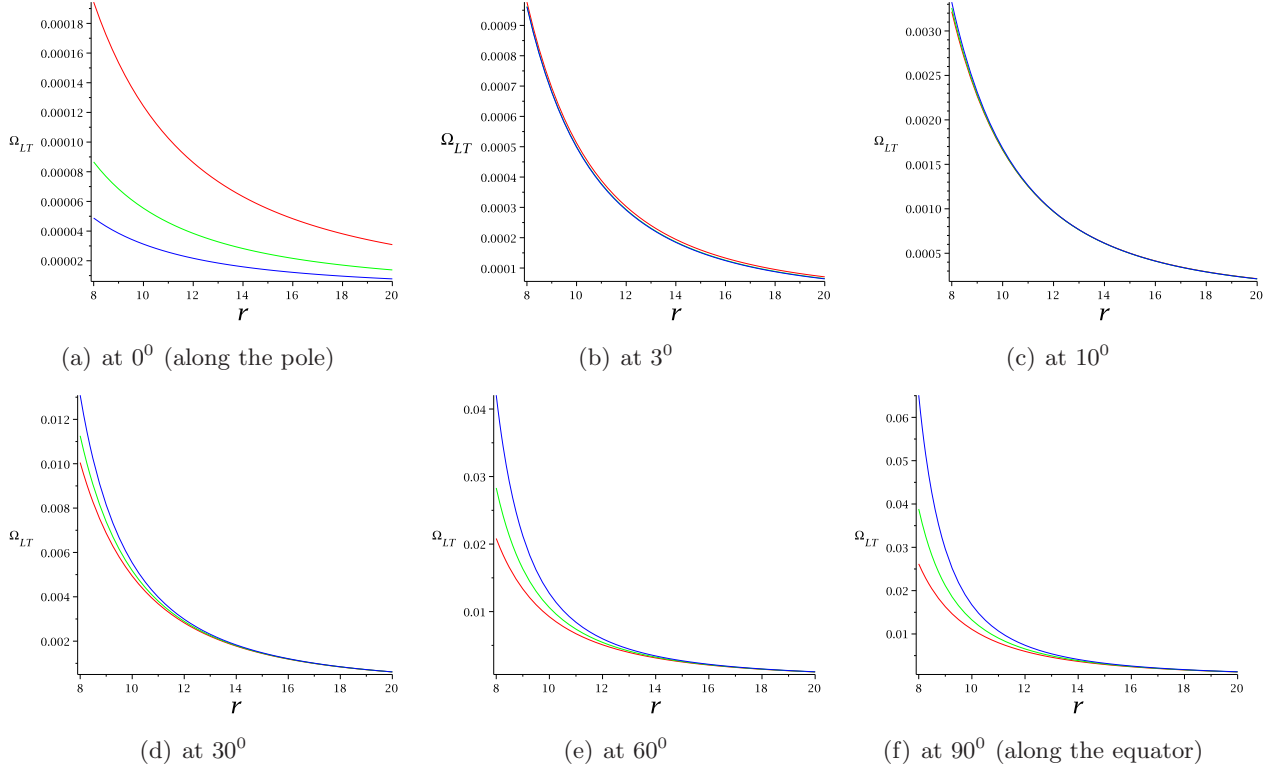


Figure 5: Plot of  $\Omega_{LT}$  vs  $r$  in the wormhole spacetime for  $b = 1$  &  $d = 1$ . Red, Green and Blue stand for  $a = 10, a = 15$  and  $a = 20$  respectively.

( $\Omega_{LT} \propto a/r^3$ ) which is evident from the Eq.(74) and Eq.(75). In the slow rotation approximation ( $r \gg \sqrt{a}$ ) these two equations reduce to

$$|\Omega_{LT}|_{\theta=0}^{slow} \approx \frac{2a}{r^3} \quad (78)$$

and

$$|\Omega_{LT}|_{\theta=\pi/2}^{slow} \approx \frac{a}{r^3} \quad (79)$$

respectively, which is expected. Even in slowly rotating Kerr spacetime, LT precession rate of a test gyro reduce to  $2a/r^3$  along the pole and  $a/r^3$  along the equator. That is why, in the slow rotation limit  $\Omega_{LT} \propto a$  and  $\Omega_{LT} \propto r^{-3}$  in the case of all compact objects as well as in the wormholes. But, in the case of a rapidly rotating wormhole  $r < \sqrt{a}$ , Eq.(74) and Eq.(75) reduce to<sup>2</sup>

$$|\Omega_{LT}|_{\theta=0}^{fast} \approx \frac{1}{8ar^2} \quad (80)$$

and

$$|\Omega_{LT}|_{\theta=\pi/2}^{fast} \approx \frac{3a}{r^3} \left(1 - \frac{b}{r}\right)^{\frac{1}{2}} \quad (81)$$

respectively. It is evident from Eq.(80) that  $\Omega_{LT}$  along the pole is proportional to  $a^{-1}$  instead of  $a$  and this adverse effect nullifies at the distance  $r \sim 16a^2$  (using Eq.(78) and Eq.(80)) along the pole. It is also surprising that  $\Omega_{LT}$  is proportional to  $r^{-2}$  instead of  $r^{-3}$  along the pole. This anomaly exists only along the pole of the wormhole and this anomaly vanishes very quickly as we move from the pole to the equator. We can see from Eq.(81) that there is no anomaly in the expression of  $\Omega_{LT}$

<sup>2</sup>we have taken  $d = 1$  [28, 21]

along the equator where  $\Omega_{LT}$  varies with  $a/r^3$  as usual. It is also seen from the plots (Fig.5) that the value of the LT precession rate along the pole is quite lower than its value along the equator. Thus, if anybody want to travel through the wormhole, she does not feel the higher dragging rate (relative to the dragging rate along the equator) due to the frame-dragging effect, even if the wormhole rotates very fast as the rapidly rotating wormhole drags its nearby spacetime ( $r < \sqrt{a}$ ) more slowly.

This same anomaly should not be appeared in case of the Kerr black hole or other axisymmetric spacetimes like other black holes and pulsars. In the Kerr spacetime, ergoregion exists at  $r_+ = M + \sqrt{M^2 - a^2/M^2 \cos^2 \theta}$  where  $a$  can take value from 0 to  $M^2$  ( $0 < a \leq M^2$ ). Thus, if we take the limit  $r < \sqrt{a}$  (Eq.(42) of [35]), it will be inside the ergoregion, which is unphysical and also beyond the frame-dragging formulation as it is valid only in the timelike region, we mean, outside the ergoregion. Thus, we cannot consider the region  $r < \sqrt{a}$  which is basically invalid and the region is inside the ergosphere. In the case of the wormhole, there is no any horizon and the LT formulation is valid for the range  $r > \sqrt{2a \sin \theta}$ . Now for  $\theta = 0$ , the LT formulation is valid in  $r > 0$  along the pole and for  $r > \sqrt{2a}$  along the equator and so on. Thus, it is meaningful to calculate the LT precession rate for any real distance greater than the throat radius ( $r > b$ ) along the pole of the wormhole spacetime. In this situation, if we calculate the LT precession rate for the region  $b < r \sim \sqrt{a}$  from Eq.(73), we can see that the LT precession rate decreases with increasing the rotation of the wormhole spacetime but this treatment is not applicable for all the angles as  $r$  must be greater than  $\sqrt{2a \sin \theta}$ .

It should be mentioned here that we had found an ‘anomaly’ in LT precession in Kerr-Taub-NUT spacetime [38] and inside the pulsars [37] where LT precession does not always follow the inverse cube law of distance but the LT precession is proportional to the rotation of those spacetime everywhere. This is first time when we have found a completely different ‘anomaly’ in the LT precession, which is related to the intrinsic rotation of a spacetime.

## 5 Discussion:

In this article, we have explored the geodesic structure of a certain class of spinning traversable Lorentzian wormholes. Likely black hole, wormhole is a solution of the Einstein equation and may be regarded as another compact object. They could be often viewed as an intrinsically topological objects. Interestingly, the ISCO equation could not be determined for the co-rotating orbit in Teo’s wormhole as the angular momentum vanishes for this prograde rotation but for the retrograde orbit there exists ISCO which coincides with the throat. One can compare it with the case of the extremal Kerr black hole(BH) [29] where the direct ISCO occurs at

$$r_{ISCO} = M, \mathcal{E}_{ISCO} = \frac{1}{\sqrt{3}}, \ell_{ISCO} = \frac{2M}{\sqrt{3}}. \quad (82)$$

and for retrograde orbit ISCO occurs at

$$r_{ISCO} = 9M, \mathcal{E}_{ISCO} = \frac{5}{3\sqrt{3}}, \ell_{ISCO} = -\frac{22M}{3\sqrt{3}}. \quad (83)$$

But in the case of Teo’s wormhole, the ISCO for the retrograde rotation exists at

$$r_{ISCO} = b, \mathcal{E}_{ISCO} = \frac{b^4 - 12a^2}{b^2 \sqrt{b^4 - 36a^2}}, \ell_{ISCO} = -\frac{6ab}{\sqrt{b^4 - 36a^2}}. \quad (84)$$

where  $b$  must be greater than  $\sqrt{6a}$  ( $b > \sqrt{6a}$ ). Otherwise,  $\mathcal{E}_{ISCO}$  and  $\ell_{ISCO}$  will be imaginary which are unphysical. Here,  $\mathcal{E}_{ISCO}$  and  $\ell_{ISCO}$  are the energy and angular momentum of the test particle which moves along the ISCO. Next we have derived the fundamental frequencies of the test particle which rotates in an equatorial circular orbit in this rotating wormhole. Finally, we have shown that the Lense-Thirring precession frequency is not to be always proportional to the rotation of the spacetime. It can also varies inversely with the angular momentum of the spacetime in some particular cases, mainly, for those spacetimes where event horizon does not exist at all. In this regard, it would be



worth to study the LT precession for the super-Kerr spacetime and also for the axially-symmetric naked singularity. Though the LT precession rate never varies inversely with the rotation of the spacetime in the Kerr black hole as it should always be proportional to the angular momentum of the spacetime but contrary to this, LT precession may act differently in the super-Kerr spacetime like the wormhole. This may help us to distinguish between the rotating Kerr black holes and the naked singularities by the astrophysical observation.

## References

- [1] A. Einstein, N. Rosen, *Phys. Rev.* **48**, 73 (1935).
- [2] J. A Wheeler, *Geometrodynamics*, Academic, New York, (1962).
- [3] M. S. Morris, K. S. Thorne, *Am. J. Phys.* **56**, 395 (1998).
- [4] M. S. Morris, K. S. Thorne, U. Yurtsever, *Phys. Rev. Lett.* **61** (13) 1446 (1988).
- [5] M. Visser, *Phys. Rev. D* **391** 3182 (1989).
- [6] V. P. Frolov and I. D. Novikov, *Phys. Rev. D* **42** 1057 (1990).
- [7] S. W. Hawking, *Phys. Rev. D* **37**, 904 (1988).
- [8] K. S. Thorne, *Black Holes and Time Warps*, W. W. Norton (1994).
- [9] R. Ian H., Wai-Mo Suen, *Phys. Rev. D* **49** (10) 5199 (1994).
- [10] M. Visser, *Phys. Rev. D* **43** 402 (1991).
- [11] D. Hochberg, A. Popov and S. V. Sushkov1, *Phys. Rev. Lett.* **78** 2050 (1997).
- [12] I. D. Novikov, *Sov. Phys. JETP* **68** 439 (1989).
- [13] J. Friedman, M. S. Morris, I. D. Novikov, F. Echeverria, G. Klinkhammer, K. S. Thorne, and U. Yurtsever, *Phys. Rev. D* **42** 1915 (1990).
- [14] M. Visser, *Nucl. Phys. B* **328** 203 (1989).
- [15] A. A. Kirillov, E. P. Savelova, *Physics Letters B* **660** (3) 93 (2008).
- [16] E. Rodrigo, *International Journal of Modern Physics D* **18**, 1809 (2009).
- [17] T. A. Roman, *Phys. Rev. D* **47** 1370 (1993).
- [18] S. Kar, *Phys. Rev. D* **49** 862 (1994).
- [19] S. Kar and D. Sahdev, *Phys. Rev. D* **53** 722 (1996).
- [20] F. Schein and P. C. Aichelburg, *Phys. Rev. Lett.* **77** 4130 (1998).
- [21] N. Tsukamoto, C. Bambi, *Phys. Rev. D* **91**, 084013 (2015).
- [22] D. Hochberg and M. Visser, *Phys. Rev. D* **58** 044021 (1998).
- [23] D. Hochberg and M. Visser, *Phys. Rev. Lett.* **81** 746 (1998).
- [24] S. W. Hawking, G. F. R. Ellis, *The Large Scale Structure of Space-time*, Cambridge University Press, Cambridge, England, (1973).
- [25] P. G. Nedkova, V. K. Tinchev, and S. S. Yazadjiev, *Phys. Rev. D* **88**, 124019 (2013).

- [26] J. G. Cramer, R. L. Forward, M. S. Morris, M. Visser, G. Benford and G. A. Landis, *Phys. Rev. D* **51**, 3117 (1995).
- [27] M. Zhou et al., *arXiv:1603.07448v1* [gr-qc] (2016).
- [28] E. Teo, *Phys. Rev. D* **58**, 024014 (1998).
- [29] S. Chandrasekhar, *The Mathematical Theory of Black Holes*, Clarendon Press, Oxford (1983).
- [30] R. M. Wald, *General Relativity*, University of Chicago Press, Chicago, (1984).
- [31] D. D. Doneva et al., *Phys. Rev. D* **90**, 044004 (2014).
- [32] J. Lense, H. Thirring, *Phys. Z.* **19**, 156-163 (1918)
- [33] L. I. Schiff, *American Journal of Physics* **28**, 340(1960)
- [34] C. W. F. Everitt et. al., *Phys. Rev. Lett.* **106**, 221101 (2011)
- [35] C. Chakraborty, P. Majumdar, *Class. Quantum Grav.* **31**, 075006 (2014).
- [36] C. Chakraborty, P. Pradhan, *Eur. Phys. J. C* **73**, 2536 (2013).
- [37] C. Chakraborty, K. P. Modak, D. Bandyopadhyay, *Astrophys. J.* **790**, 2 (2014).
- [38] C. Chakraborty, *Eur. Phys. J. C* **75**, 572 (2015)